The Effects of Measurement Noise on Vehicle Motion Control with Delayed State Feedback

Illés Vörös* and Dénes Takács*,†
*Department of Applied Mechanics, Budapest University of Technology and Economics, Budapest, Hungary
†MTA-BME Research Group on Dynamics of Machines and Vehicles

Summary. The stability properties of the single track vehicle model with proportional, delayed feedback control are investigated in the presence of measurement noise. The moment stability and the stationary behavior of the resulting stochastic system is analyzed using the stochastic semi-discretization method and numerical simulations are conducted to verify the results.

Introduction

The stabilization of path following is a fundamental element of numerous autonomous driving functions from lane keeping to self-driving. The focus of this work is to investigate the effects of measurement noise in the feedback loop of a path following controller with time delay, leading to a system of stochastic delay differential equations (SDDE's).
A number of important results have been developed over the years for the analysis of such systems. The moment stability of the solution in the linear case was presented in [1]. In [2], an approximate Fokker-Planck equation was introduced for the stationary solutions of nonlinear SDDE's with small delays. The stability of linear control systems with time delay was investigated in [3] using the Lyapunov exponent approach. The Taylor expansion of the control force was used in [4] and [5] to investigate the control of stochastic time delay systems in the linear and the non-linear case, respectively.
In this paper, the stochastic semi-discretization method [6] is used in order to determine the second moment of the stationary solution of a path following controller with time delay and measurement noise. Due to the so-called autonomous stochastic resonance phenomenon, the effects of the noise excitation may be amplified close to the stability boundaries, leading to an exceedingly large variance of the system response even if the control gains are selected from the stable parameter domain. The stochastic semi-discretization method generates a mapping of the discretized second moment, which can be used to assess the stability properties and the steady state solution of the second moment dynamics. As a result, specific regions of the control gains can be established within the stable domains that correspond to a given maximum allowable variance of the solution.
The rest of the paper is organized as follows: the mathematical model of the closed-loop system is introduced first. The second moment of the stationary solution is analyzed along the stable domain of control parameters with the help of the stochastic semi-discretization method and the results are verified by numerical simulations of the linear system. Next, the effects of a cutoff frequency in the measurement noise are investigated, then numerical simulations are also performed on the non-linear system by applying filtered white noise.

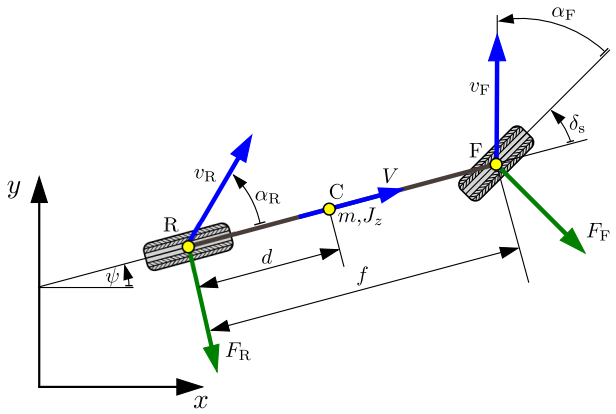

Figure 1: The single track vehicle model

Vehicle model

The mechanical model of our analysis is based on the single track vehicle model (see Fig. 1) with linear tire characteristics, according to [7]. Linearizing the system around the rectilinear motion along the x axis leads to the linear system $\dot{\mathbf{x}}(t) = \mathbf{A}\mathbf{x}(t) + \mathbf{B}\delta_s(t)$, where the state vector $\mathbf{x} = \begin{bmatrix} y & \psi & \sigma_1 & \sigma_2 \end{bmatrix}^T$ includes the lateral position, yaw angle, lateral velocity

Table 1: Parameter values used for stability maps and simulations

f (m)	d (m)	m (kg)	J_z (kgm^2)	C_F (N/rad)	C_R (N/rad)	V (m/s)	τ (s)	σ_y (m)	σ_ψ (rad)
2.7	1.35	1430	2500	45000	45000	20	0.5	0.1	0.005

and yaw rate of the vehicle, respectively. The steering angle is denoted by δ_s, while the system and input matrices are

$$\mathbf{A} = \begin{bmatrix} 0 & V & 1 & 0 \\ 0 & 0 & 0 & 1 \\ 0 & 0 & A_{33} & A_{34} \\ 0 & 0 & A_{43} & A_{44} \end{bmatrix} \quad \text{and} \quad \mathbf{B} = \begin{bmatrix} 0 \\ 0 \\ B_3 \\ B_4 \end{bmatrix} \tag{1}$$

with the elements

$$\begin{gathered} A_{33} = -\frac{B_3}{V} - \frac{C_\mathrm{R}(J_z + md^2)}{mVJ_z}\,, \quad A_{34} = -B_3\frac{f}{V} - V\,, \quad B_3 = \frac{C_\mathrm{F}(J_z + md(d-f))}{mJ_z}\,, \\ A_{43} = -\frac{B_4}{V} + \frac{C_\mathrm{R}d}{VJ_z}\,, \quad A_{44} = -B_4\frac{f}{V}\,, \quad B_4 = \frac{C_\mathrm{F}(f-d)}{J_z}\,. \end{gathered} \tag{2}$$

The vehicle parameters include the mass m, the yaw moment of inertia J_z (with respect to the center of gravity), the wheelbase f, and the distance d between the rear axle and the center of gravity. V denotes the longitudinal speed of the vehicle (assumed to be constant), and the tire cornering stiffnesses are denoted by C_F (front axle) and C_R (rear axle). The control goal is to reach stable rectilinear motion along the x axis, therefore the steering angle is generated by the delayed feedback of the vehicle's lateral position y and its yaw angle ψ: $\delta_\mathrm{s}(t) = \mathbf{K}\mathbf{x}(t-\tau) = -P_y y(t-\tau) - P_\psi \psi(t-\tau)$, where $\mathbf{K} = \begin{bmatrix} -P_y & -P_\psi & 0 & 0 \end{bmatrix}$ includes the control gains. The time delay τ consists of sensor and communication delays, processing times, as well as the dynamics of the steering mechanism.

In order to represent measurement noise in the control loop, the above model is extended by adding an additive noise component to the feedback signal of both y and ψ. This may include effects from environmental noise or the slight jumps in the estimation results of the lane detection system in each frame in case of a vision-based solution. The noise is modeled as a one-dimensional Langevin force excitation Γ_t [9], with the intensities σ_y and σ_ψ collected in $\mathbf{D}_\mathrm{m} = \begin{bmatrix} \sigma_y & \sigma_\psi & 0 & 0 \end{bmatrix}^\mathrm{T}$. Overall, the resulting linear, stochastic, time delay system can be written as

$$\dot{\mathbf{x}}(t) = \mathbf{A}\mathbf{x}(t) + \mathbf{B}\mathbf{K}\mathbf{x}(t-\tau) + \boldsymbol{\sigma}\Gamma_t\,, \quad \text{where} \quad \boldsymbol{\sigma} = \mathbf{B}\mathbf{K}\mathbf{D}_\mathrm{m}\,. \tag{3}$$

Since the Langevin force excitation Γ_t is defined such that its integration leads to the Wiener process W_t [9], Eq. (3) can be rewritten into the incremental form

$$\mathrm{d}\mathbf{x}(t) = (\mathbf{A}\mathbf{x}(t) + \mathbf{B}\mathbf{K}\mathbf{x}(t-\tau))\,\mathrm{d}t + \boldsymbol{\sigma}\mathrm{d}W_t\,. \tag{4}$$

Stability analysis

The system may lose its stability in two ways: at $P_y = 0$, a static loss of stability occurs, which corresponds to a real characteristic root crossing the imaginary axis. At the rest of the stability boundaries, a complex conjugate pair of roots moves to the right half-plane, leading to an oscillatory loss of stability. The analytical derivation of these stability boundaries for the deterministic system using the D-subdivision method is detailed in [7].

In order to investigate the stability properties of the stochastic delay differential equation (4), the stochastic mapping $\mathbf{y}_{n+1} = \mathbf{F}\mathbf{y}_n + \mathbf{g}$ is defined by discretizing the system with respect to the delayed term [6, 8]. The size of $\mathbf{y}_n$ depends on the resolution of the discretization; $\mathbf{F}$ is based on the deterministic part of Eq. (4) ($\mathbf{A}$ and $\mathbf{BK}$), and $\mathbf{g}$ is calculated from $\boldsymbol{\sigma}$. For the exact definition of the above mapping, the reader is referred to [6].

The stability of the mean dynamics is determined by $\mathbf{F}$ (leading to the results presented in [7]), while the second moment stability is analyzed according to [6]. Note that first moment stability is required for the stability of the second moment process, therefore it is sufficient to check only the latter. Moreover, since there is no multiplicative noise term in our model, stability analysis of the first and second moment dynamics leads to the same results. In other words, the introduction of additive sensor noise does not influence the stability boundaries of the system. However, due to the autonomous stochastic resonance effect, the steady-state second moment values may start to increase near the stability boundaries. This means that even though the control gains are chosen from the stable parameter domain, the variance of the steady state solution may become unacceptably large.

In order to check this, the first order stochastic semi-discretization method was applied with the help of the corresponding Julia package [6]. A discretization step of 0.05 s was used and the vehicle parameters were selected according to Table 1. The effect of autonomous stochastic resonance is illustrated in Fig. 2 (a), where the steady state second moment of y (denoted by $M_{\mathrm{st},y}$) is plotted along the stable parameter domain of the control gains. The sections of the stability map were chosen according to the control gains that lead to the most highly damped response of the deterministic system ($P_y = 0.00077$ m^{-1}, $P_\psi = 0.0805$).

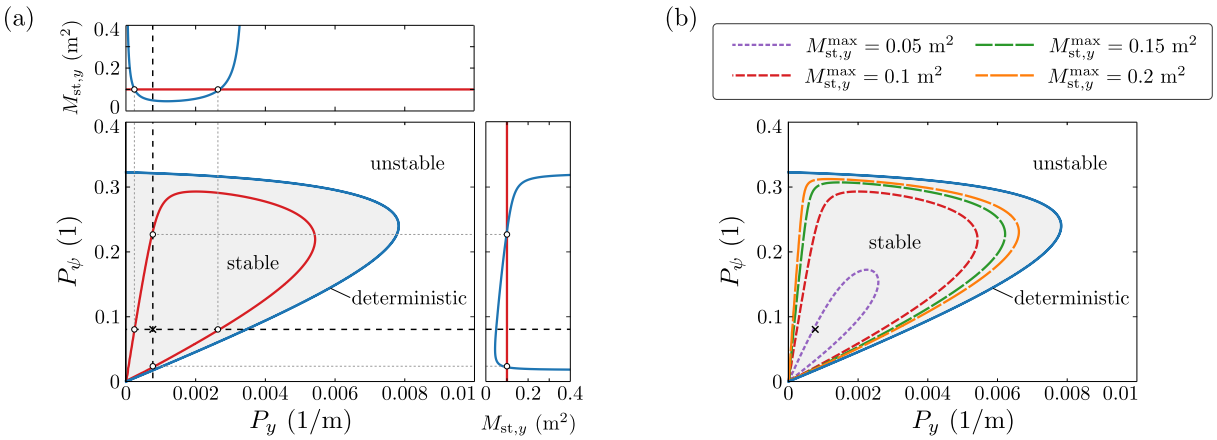

Figure 2: (a) The effect of sensor noise on the steady state second moment of y; (b) regions of the stability map corresponding to different limits on $M_{\mathrm{st},y}$; the deterministic optimum is denoted with a cross

Figure 2 (b) shows a practical stability map that demonstrates how the usable domain of control parameters shrinks if we want to limit the steady state second moment of y. Notice that the minimum of $M_{\mathrm{st},y}$ does not fall into the deterministic optimum (that is based on the eigenvalues of $\mathbf{F}$). Instead, it depends on the values of σ_y and σ_ψ, and the amplification due to the control gains.

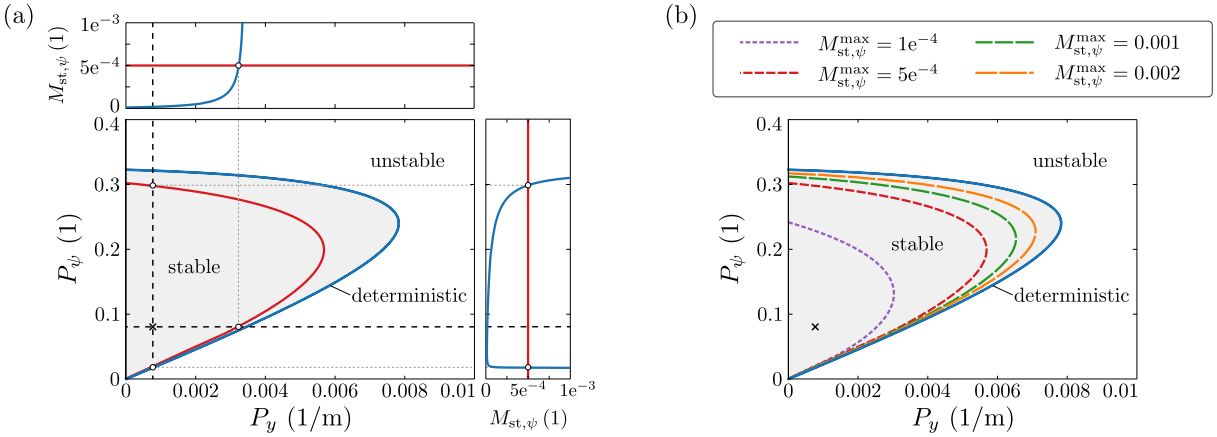

Figure 3: (a) The effect of sensor noise on the steady state second moment of ψ; (b) regions of the stability map corresponding to different limits on $M_{\mathrm{st},\psi}$; the deterministic optimum is denoted with a cross

Figure 3 shows similar practical stability maps with regards to the steady state second moment of the yaw angle ψ. Note the different shape of the contour lines compared to those in Fig. 2. As P_y is decreased, the vehicle takes much longer to reach the equilibrium (in terms of mean dynamics), since the position error is very weakly compensated (at $P_y = 0$, a static loss of stability occurs, where the vehicle path diverges). This also means that the steering action does not suppress the stochastic jumps around the equilibrium as effectively once the steady state is reached, leading to an increase in $M_{\mathrm{st},y}$ (as seen in Fig. 2 (a)). On the other hand, the control action related to ψ is not affected as P_y is decreased, which explains why there is no increase in $M_{\mathrm{st},\psi}$ in Fig. 3 (a) (note that $M_{\mathrm{st},\psi}$ does not reach zero at $P_y = 0$). Another effect to keep in mind, however, is that decreasing the gains not only decreases the control action, but it also suppresses the noise amplitude that appears in δ_{s}. Therefore decreasing the control gains directly leads to decreased noise gains, which means that the second moments are generally lower near the origin of the stability maps (unless of course stochastic resonance effects appear due to the proximity of a stability boundary).

In order to verify the results, 1000 Monte-Carlo simulation runs were conducted using the Euler-Maruyama method [10]. The control gains were chosen according to the deterministic optimum, and an initial condition of $y(t \leq 0) = 3\,\mathrm{m}$ was used (while the rest of the initial state values were set to zero), representing a lane change manoeuvre. The simulations were run for 100 seconds, with a time step of $0.005\,\mathrm{s}$. In order to calculate the stationary second moment, the first 30 seconds of the simulations were cut to ensure proper decay of the transients. There is good accordance between the numerically determined stationary second moment and the result of the stochastic semi-discretization method (see the first two columns of Table 2). This is also illustrated in Fig. 4, where the square root of the stationary second moment according to the semi-discretization method (shown in red) matches the sample standard deviation of the Monte-Carlo runs (shown in blue; note that the expected value of the stationary solution is zero).

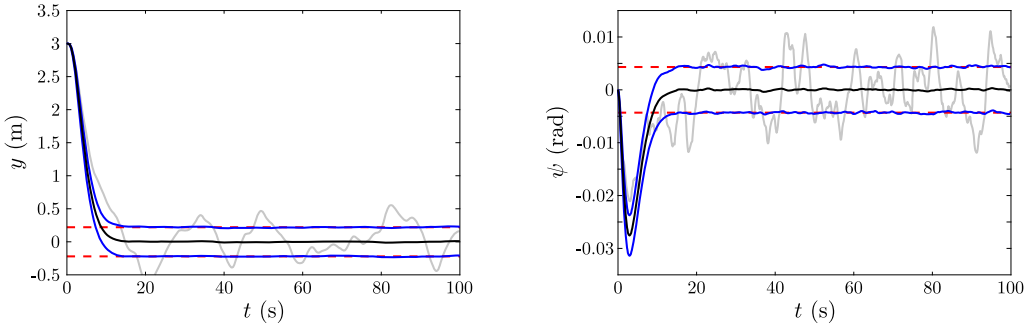

Figure 4: Simulation results of 1000 Monte-Carlo runs of the linear system. Black lines show the sample mean and blue lines denote the standard deviations of the samples. An arbitrarily chosen single realization is shown in light gray, while the red dashed lines represent the square root of the stationary second moments calculated using stochastic semi-discretization.

Table 2: Stationary second moment values determined using different methods

	Stochastic SD	Linear simulation	Non-linear simulation
$M_{\mathrm{st},y}$ (m^2)	0.04867	0.04783	0.04896
$M_{\mathrm{st},\psi}$ (rad^2)	1.8642e-5	1.8553e-5	1.8741e-5

Colored noise, simulation of the nonlinear system

A possible extension of the previously detailed model is the use of colored noise in the form of a first order Markov process [11]. This approach incorporates a cutoff frequency ω_{c} to limit the bandwidth of measurement noise due to e.g. digitization. The noise processes corresponding to the feedback signal of y and ψ are

$$\dot{w}_y = -\frac{1}{T_y} w_y + \sigma_y^{\mathrm{c}} \Gamma_t \,, \qquad \dot{w}_\psi = -\frac{1}{T_\psi} w_\psi + \sigma_\psi^{\mathrm{c}} \Gamma_t \,, \tag{5}$$

where w_i ($i \in \{y, \psi\}$) denote the state of the noise process and the time constants T_i determine the correlation time of the noise and the corresponding cutoff frequency ($\omega_{\mathrm{c}} = 1/T_i$). This time constant is assumed to be equal for both measurement signals.
As opposed to the previous section, the Langevin force excitation Γ_t is now used to generate the colored noise process, instead of directly acting on the feedback signal. Its intensity σ_i^{c} is chosen such that the energy content of the colored noise process (at low frequency levels) matches the corresponding white noise process used in the previous section, leading to

$$(\sigma_i^{\mathrm{c}})^2 = \frac{\sigma_i^2}{T_i^2} \,, \qquad i \in \{y, \psi\} \,. \tag{6}$$

Using the above noise processes, the closed-loop system is of the form

$$\dot{\mathbf{x}}(t) = \mathbf{A}\mathbf{x}(t) + \mathbf{B}\mathbf{K} \left(\mathbf{x}(t-\tau) + \mathbf{D} \begin{bmatrix} w_y \\ w_\psi \end{bmatrix} \right) \,, \qquad \mathbf{D} = \begin{bmatrix} 1 & 0 & 0 & 0 \\ 0 & 1 & 0 & 0 \end{bmatrix}^{\mathrm{T}} \,. \tag{7}$$

Combining Eq. (5) and Eq. (7), the system can be turned to a similar form as Eq. (3)

$$\dot{\mathbf{X}}(t) = \left[\begin{array}{c|cc} \mathbf{A} & \multicolumn{2}{c}{\mathbf{BKD}} \\ \hline \mathbf{0}_{2,4} & -1/T_y & 0 \\ & 0 & -1/T_\psi \end{array}\right] \mathbf{X}(t) + \left[\begin{array}{c|c} \mathbf{BK} & \mathbf{0}_{4,2} \\ \hline \mathbf{0}_{2,4} & \mathbf{0}_{2,2} \end{array}\right] \mathbf{X}(t-\tau) + \left[\begin{array}{cc} \mathbf{0}_{4,2} & \\ \hline \sigma_y^{\mathrm{c}} & 0 \\ 0 & \sigma_\psi^{\mathrm{c}} \end{array}\right] \Gamma_t \tag{8}$$

using the augmented state vector

$$\mathbf{X} = \begin{bmatrix} y & \psi & \sigma_1 & \sigma_2 & w_y & w_\psi \end{bmatrix}^{\mathrm{T}} \,. \tag{9}$$

$\mathbf{0}_{i,j}$ represents the zero matrix of size $i \times j$.
The stability maps in Fig. 5 demonstrate how the cutoff frequency of the measurement noise affects the previously shown robust stability maps. At the boundary of dynamic loss of stability (the so-called D-curve), a complex conjugate pair of characteristic roots crosses the imaginary axis at $\mathrm{i}\omega$. The value of ω continuously increases along the stability boundary from $\omega = 0$ at the origin to approximately $\omega = 2$ rad/s where the D-curve crosses the vertical axis slightly above $P_\psi = 0.3$. The line style of the deterministic boundary in Fig. 5 shows the relation between the selected cutoff frequency and the system dynamics. The section of the stability boundary where the imaginary part of the corresponding characteristic roots is below the cutoff frequency is shown in blue, while the sections plotted in dashed gray are above ω_{c}.

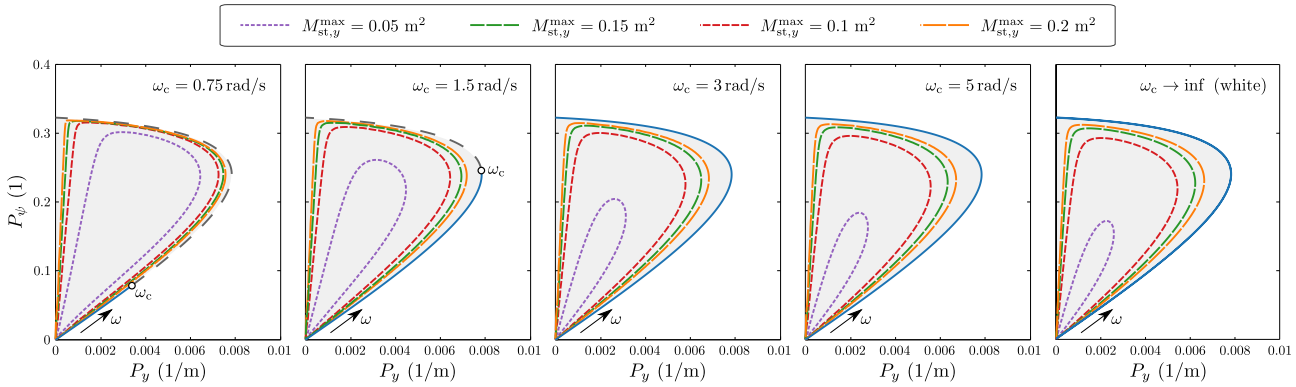

Figure 5: Robust stability maps in terms of the steady state second moment of y while increasing the cutoff frequency of the sensor noise (ω_c). The styling of the deterministic boundary shows the relation between the frequency component ω of the critical characteristic roots at the boundary and the cutoff frequency ω_c (blue: $\omega < \omega_c$, gray dashed: $\omega > \omega_c$).

It can be seen that as long as only a small section of the stability boundary (and therefore the corresponding dynamics) is excited, the stochastic resonance effect is not very strong, the stationary second moment of y remains small throughout the majority of the stable parameter domain, and there is not much difference between the deterministic and the robust stability boundaries. However, as the cutoff frequency is increased, the stochastic excitation has a stronger effect on the dynamics, and the contour lines of $M_{\mathrm{st},y}$ start tending towards those shown for white noise excitation. Since the vehicle model acts as a low-pass filter with relatively slow dynamics, the colored sensor noise also has to have a very low cutoff frequency in order to show a meaningful difference in terms of the steady-state dynamics of the system compared to a white noise excitation. Therefore there is not much benefit in taking into account the cutoff frequency of the sensor noise in most practical cases, where ω_c is typically at least 10 Hz.

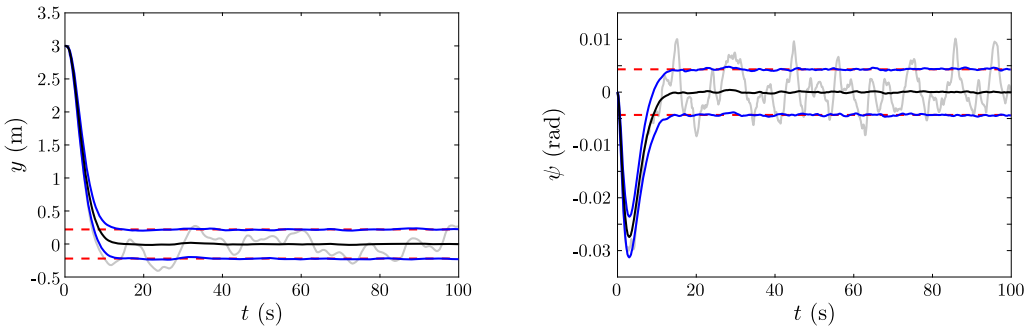

Figure 6: Simulation results of 1000 Monte-Carlo runs of the non-linear system. Black lines show the sample mean and blue lines denote the standard deviations of the samples. An arbitrarily chosen single realization is shown in light gray, while the red dashed lines represent the square root of the stationary second moments calculated using stochastic semi-discretization.

On the other hand, a possible advantage of modeling the additive sensor noise as a first order Markov process is that this approach allows the numerical simulation of the non-linear system too (the non-linear system equations can be found in [7]). In spite of feeding back the measurement noise through non-linear functions, the overall system remains driven by an additive, white noise source, which is easy to handle mathematically.
The results in Fig. 6 and Table 2 show that there is minimal difference in the observed stationary second moments between performing simulations on the linear and the non-linear system. This is mainly due to the fact that only geometrical non-linearities are considered, which do not have a strong effect in the performed lane change manoeuvre, especially once the steady state is reached. Even though there is constant steering action due to the stochastic effects, the steering and side-slip angles all remain small enough that the system stays well within the linear regime. Nevertheless, this still provides a useful example of simulating a non-linear system with direct feedback of measurement noise.

Conclusion

The stability and steady-state dynamics of a path tracking controller were investigated in the presence of time delay and measurement noise. It was shown how the choice of control parameters influences the steady-state dynamics. Due to the autonomous stochastic resonance effect, it is possible to choose control gains from the linearly stable parameter domain that still lead to unacceptably large variance in the steady-state solution. The included robust stability maps aim to provide guidelines about which regions of the stable domain should be avoided for this reason. The results determined using the stochastic semi-discretization method were verified by numerical simulations. The simulation of the non-linear stochastic system was achieved by using filtered white noise. A possible extension of the present study is to also consider the effects of road excitation as another noise source in the system.

Acknowledgment This research was partly supported by the National Research, Development and Innovation Office under grant no. NKFI-128422 and by the Higher Education Excellence Program of the Ministry of Human Capacities in the frame of Artificial intelligence research area of Budapest University of Technology and Economics (BME FIKP-MI). The authors would like to thank Henrik Sykora for his valuable comments.

References

[1] Mackey M. C., Nechaeva I. G. (1995) Solution moment stability in stochastic differential delay equations. *Physical Review E* **52**(4):3366-3376.

[2] Guillouzic S., L'Heureux I., Longtin A. (1999) Small delay approximation of stochastic delay differential equations. *Physical Review E* **59**(4):3970-3982.

[3] Grigoriu M. (1997) Control of time delay linear systems with Gaussian white noise. *Probabilistic Engineering Mechanics* **12**(2):89-96.

[4] Di Paola M., Pirrotta A. (2001) Time delay induced effects on control of linear systems under random excitation. *Probabilistic Engineering Mechanics* **16**(1):43-51.

[5] Bilello C., Di Paola M., Pirrotta A. (2002) Time delay induced effects on control of non-linear systems under random excitation. *Meccanica* **37**(1-2):207-220.

[6] Sykora H. T., Bachrathy D., Stépán G. (2019) Stochastic semi-discretization for linear stochastic delay differential equations. *International Journal for Numerical Methods in Engineering* **119**(9):879-898.

[7] Vörös I., Várszegi B., Takács D. (2019) Lane Keeping Control Using Finite Spectrum Assignment with Modeling Errors. *ASME 2019 Dynamic Systems and Control Conference* DSCC2019-8960.

[8] Insperger T., Stépán G. (2011) Semi-discretization for time-delay systems: stability and engineering applications. Springer Science & Business Media, New York.

[9] Øksendal B. (2003) Stochastic differential equations. Springer, Berlin, Germany.

[10] Higham D. J. (2001) An algorithmic introduction to numerical simulation of stochastic differential equations. *SIAM review* **43**(3):525-546.

[11] Maybeck P. S. (1982) Stochastic models, estimation, and control. Academic Press, New York.